IEEE Access
Multidisciplinary | Rapid Review | Open Access Journal

Received September 23, 2019, accepted October 21, 2019, date of publication October 23, 2019, date of current version November 6, 2019.

Digital Object Identifier 10.1109/ACCESS.2019.2949201

Modulation Format Identification in Mode Division Multiplexed Optical Networks

WADDAH S. SAIF[1,2], AMR M. RAGHEB[2], HUSSEIN E. SELEEM[3], TARIQ A. ALSHAWI[2], AND SALEH A. ALSHEBEILI[1,2]

[1]Electrical Engineering Department, King Saud University, Riyadh 11421, Saudi Arabia
[2]KACST-TIC in Radio Frequency and Photonics (RFTONICS), King Saud University, Riyadh 11421, Saudi Arabia
[3]Department of Electronics and Electrical Communications, Faculty of Engineering, Tanta University, Tanta 31512, Egypt

Corresponding author: Waddah S. Saif (wsaif@ksu.edu.sa)

This work was supported by the Deanship of Scientific Research, King Saud University through Research Group under Grant RG-1438-092.

ABSTRACT In this paper, we address the problem of modulation format identification (MFI) for few mode fiber (FMF) transmission in elastic optical networks (EONs). The MFI accuracy is studied under different FMF channel conditions including mode coupling (MC), optical signal-to-noise ratio (OSNR), and chromatic dispersion (CD). Artificial neural network, trained using features extracted from the asynchronous in-phase quadrature histogram (IQH), is proposed to investigate the identification accuracy. Extensive simulation results have been conducted to identify six modulation schemes widely used in polarization division multiplexing coherent optical networks. This includes PDM-BPSK, PDM-QPSK, PDM-8QAM, PDM-16QAM, PDM-32QAM, and PDM-64QAM transmitted at 10 Gbaud network transmission speed. The results show that the proposed MFI achieves a successful average identification accuracy exceeding 98% in the presence of low MC when the incoming signal OSNR is greater than 20 dB. However, the effect of high MC and CD = 1100 ps/nm reduces the average accuracy to 90%. Further, the MFI accuracy is investigated under different symbol rates such as 14 and 20 Gbaud.

INDEX TERMS Coherent optical communication, few mode fiber, modulation format identification.

I. INTRODUCTION

Machine learning (ML) has shown an intensive impact on the recent advances of the optical communication field. This includes building autonomous optical nodes, mitigating fiber nonlinearities, optimizing data centers, securing Internet of Things (IoTs) technologies, etc. In particular, modulation format identification (MFI) using ML algorithms are becoming a common need in the next generation elastic optical networks (EONs). Additionally, as the spectral efficiency in single mode fiber (SMF) based optical networks approaching the Shannon capacity limit, imposed by fiber nonlinearities, space division multiplexing (SDM) has been proposed as a candidate solution to meet the ever increasing demand of ultra-high date transmission rates [1]–[3]. Among the various techniques of SDM, few-mode fiber (FMF), known as mode-division multiplexing (MDM), improves the spectral efficiency by utilizing the orthogonal modes passing through the fiber, where each mode is treated as an individual optical channel [4]. Thus, it duplicates the channel capacity to several of terabits over long distances as well as reduces the overall cost [5], [6].

In addition to the efficient utilization of the optical physical layer and optical spectrum, the network elements are evolving to be all-optical and self-programmable. For instance, the optical add/drop multiplexers (OADMs), which are responsible of performing sophisticated signal routing, are promoted to include configurability functions [7], [8]. Hence, these elements become more agile and are able to perform software driven remote reconfiguration [9]. Furthermore, EONs are expected to be heterogeneous and adaptively supporting various modulation formats and different data rates (i.e. depend on the network operating demands and status) [10]. Therefore, the optical nodes in such networks must have the ability to automatically recognize the modulation formats at different rates without any prior information from the transmitter side.

Moreover, the seamless integration between SMFs and FMFs will definitely increase the network throughput, compared to the already deployed SMF-based networks [11].

The associate editor coordinating the review of this manuscript and approving it for publication was Tianhua Xu.

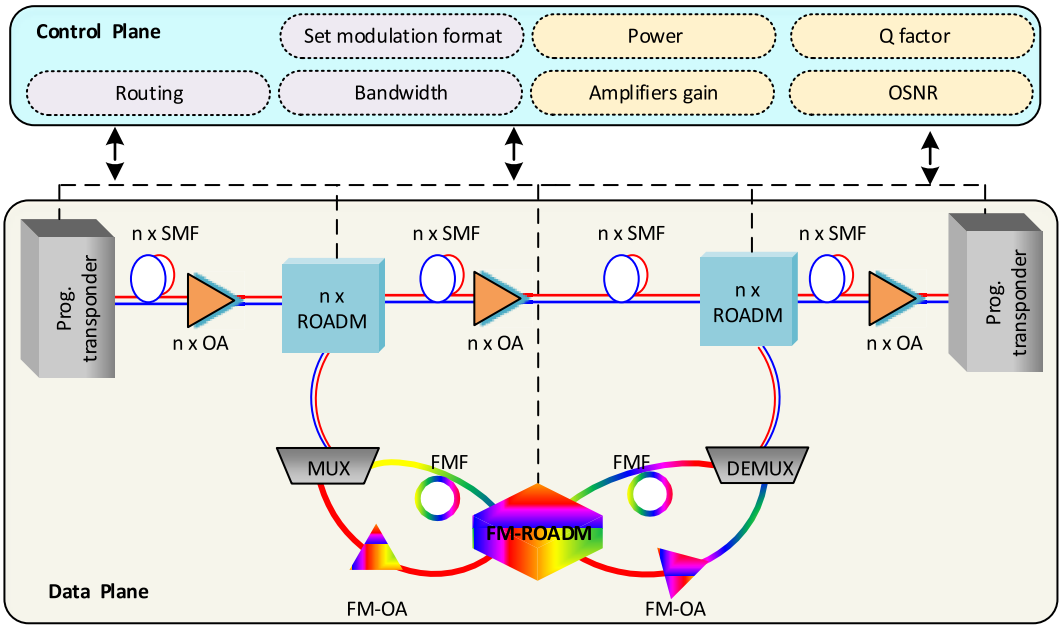

FIGURE 1. The integrated SMF/FMF SDN network architecture. SDN: software defined network, ROADM: reconfigurable optical add drop multiplexer, OA: optical amplifier, MUX: multiplexer, DEMUX: de-multiplexer, SMF: single mode fiber, FMF: few mode fiber.

Thus, ML technologies will play a significant role in order to manage, organize, and optimize such networks. In this regard, software defined networks (SDNs) provide the potential for these networks to be smart/intelligent. SDNs allocate the network resources adaptively such as modulation format, wavelength, routing path, etc. The architecture of the SDNs comprises the control plane and data plane [12]. The former is considered as the brain of the SDN system, which can be used to automate the network, while the latter plane represents the network infrastructure. In Fig. 1, we show the integrated SMF/FMF SDN network architecture where the data plane contains the network main elements such as the programmable transponders, reconfigurable OADMs (ROADMs), optical amplifiers, etc. In specific, the ROADMs cross either SMF links to add/drop network wavelengths or FMF links to add/drop the supported fiber modes. The transponders can adaptively choose the appropriate modulation format. At the control plane, the resources allocation is managed by the SDN controller, which reads the communication metrics, such as optical signal-to-noise ratio (OSNR), Q factor, etc., of each node at regular intervals. Then, it assigns the suitable modulation format to the transponders or configures the ROADMs to change the optical channel path.

On the other side, MFI in SMF-based optical networks has been investigated thoroughly in the last few years. In this regard, the asynchronous amplitude histogram (AAH) [13]–[15] and the cumulative distribution function (CDF) [16], [17] of the received samples have been exploited in the feature-based recognition algorithms. These techniques limit the recognition process to M-ary quadrature amplitude modulation (M-QAM) schemes; owing to the lack of phase information essentially needed for other schemes such as M-ary phase shift keying (M-PSK). In [18], [19], the MFI is achieved by exploiting Stokes space. Also, image processing techniques have been exploited in MFI [20], [21]. Besides, other MFI methods based on binary decision tree have been investigated in literature. This includes spectrum analysis [22], [23], amplitude deviation analysis [24], the entropy of the normalized amplitude histogram [25], and the distribution of amplitude and phase [26] of the received signal.

Nonetheless, all existing literature have focused on the MFI in SMF-based EONs. In this work, we consider the MFI in FMF-based network. Besides the traditional SMF's impairments, FMF has its own impairments that limit the communication over such type of SDM networks; an example of which is the mode coupling (MC) effect resulting from the lateral misalignment of optical connectors. Therefore, MFI is proposed for FMF network under the effect of MC, chromatic dispersion (CD), and amplified spontaneous emission (ASE) noise. Five spatial modes are considered: LP_{01}, LP_{11a}, LP_{11b}, LP_{21a}, and LP_{21b}. The modulation pool includes six formats commonly used in polarization division multiplexing (PDM) coherent optical systems, and transmitted at 10 Gbaud network speed. These formats are BPSK, QPSK, 8-QAM, 16-QAM, 32-QAM, and 64-QAM. We use an MFI technique based on feed-forward artificial neural network (ANN), trained with the asynchronous in-phase quadrature histogram (IQH), recently introduced in [27], for impairments separability investigation in SMF-based optical network. Unlike AAH, the IQH carries information about both amplitude and phase, which are exploited here for the identification of M-QAM and M-PSK modulation formats.

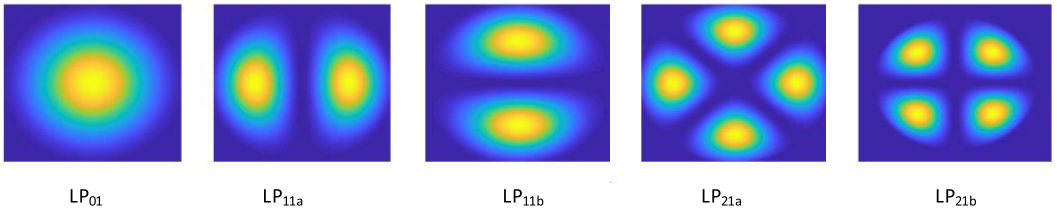

FIGURE 2. Profiles of five spatial modes.

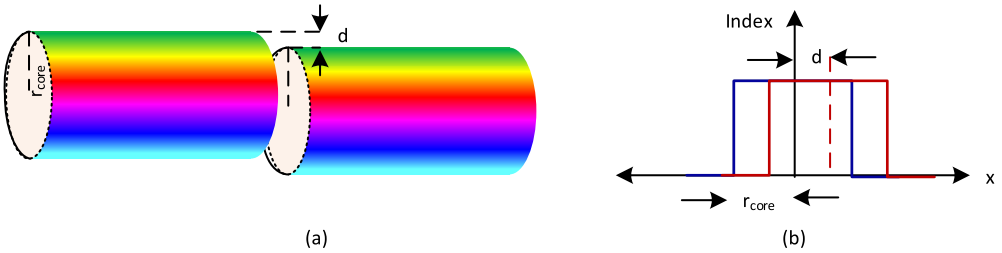

FIGURE 3. Lateral misalignment between two identical FMF: (a) geometry view, and (b) cross section view.

Simulation results show high average identification accuracy, which exceeds 98% in the presence of low MC. The impact of CD and high MC causes a decrease in the classification accuracy to 90%. Finally, the effectiveness of the proposed technique is further evaluated by examining the MFI scheme under different symbol rates such as 14 and 20 Gbaud. To the best of our knowledge, this study is the first to utilize the IQH in modulation format identification, and the first to consider modulation format identification in FMF.

II. OPERATING PRINCIPLE

A. FEW-MODE FIBER (FMF) TRANSMISSION MODEL

Optical fiber is a cylindrical wave guide with a core of high refractive index n_1 surrounded by a cladding of a low refractive index n_2. The number of guided modes propagating inside the fiber cable is determined by the normalized frequency V expressed as [28]

$$V = \frac{2\pi}{\lambda} a\sqrt{n_1^2 - n_2^2} \tag{1}$$

where a is the core radius, and λ is the operating wavelength. The guided modes are usually described as linearly polarized LP_{lp} waves, where l and p are integer numbers representing the azimuthal and radial indices, respectively. For SMF, the value of V is small (i.e. 2.405) and only the fundamental mode LP_{01} is propagating inside the fiber core. If the value of V exceeds 2.405, higher order modes can pass through the fiber such as LP_{11}, LP_{21}, etc. These modes exist inside the fiber with two different spatial orientations (e.g. in case of LP_{11}, two modes exist: even LP_{11a} and odd LP_{11b}). Figure 2 shows the mode profile of the five different spatial modes considered in this paper.

Ideally, the propagated modes inside the FMF cable are transmitted in an orthogonal manner such that each mode is not affected by the other. Let ψ_{lp} represent the modal basis of LP_{lp}, then [29]

$$\int_0^{2\pi}\int_0^{\infty} \psi_{lp}\psi_{l'p'} dr d\theta = \begin{cases} 1, & \text{if } l = l',\ p = p' \\ 0, & \text{otherwise} \end{cases} \tag{2}$$

However, in reality, the energy is coupled between the coexisting modes. This effect is known as MC. MC can occur either in the transmission medium itself [30], [31] or at the fiber connections [29]. This causes a crosstalk between the spatially multiplexed signals. Note that, MC can be mitigated using multi-input multi-output (MIMO) processing algorithms [32], [33], at the receiver side. The MC between the different spatially multiplexed modes can be expressed as [29]

$$\mathbf{a_{out}} = \mathbf{C}\,\mathbf{a_{in}} \tag{3}$$

where $\mathbf{a_{in}}$ and $\mathbf{a_{out}}$ are the input and output mode vectors, respectively, and $\mathbf{C}$ is the coupling matrix given by

$$\mathbf{C} = \begin{bmatrix} c_{01-01} & c_{11a-01} & c_{11b-01} & c_{21a-01}\cdots \\ c_{01-11a} & c_{11a-11a} & c_{11b-11a} & c_{21a-11a}\cdots \\ c_{01-11b} & c_{11a-11b} & c_{11b-11b} & c_{21a-11b}\cdots \\ c_{01-21a} & c_{11a-21a} & c_{11b-21a} & c_{21a-21a}\cdots \\ c_{01-21b} & c_{11a-21b} & c_{11b-21b} & c_{21a-21b}\cdots \\ \vdots & \vdots & \vdots & \vdots \end{bmatrix} \tag{4}$$

where the matrix element c_{i-j} is the coupling coefficient between the i^{th} and j^{th} modes. The diagonal elements represent the self-coupling (or transmission) coefficients while the rest matrix elements represent the cross-coupling coefficients. In this paper, we consider the mode coupling arising from fiber cable connections. Thus, the coupling between modes results from the misalignment between connectors/splices, as shown in Fig. 3. The normalized misalignment distance D is given by [29]

$$D = \frac{d}{r_{core}} \tag{5}$$

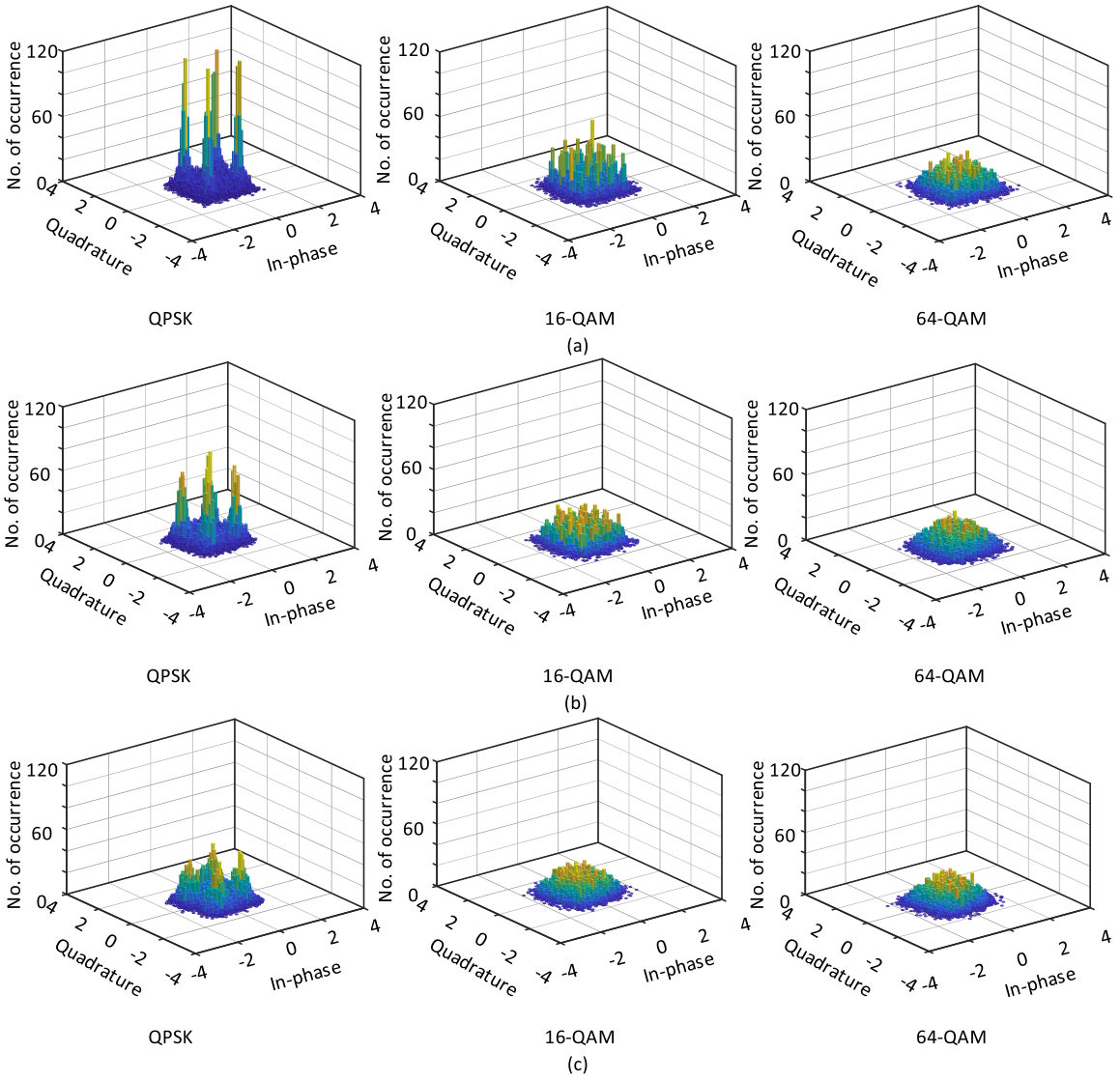

FIGURE 4. IQH for different modulation formats at OSNR = 36 dB and data rate = 10 Gbaud: (a) Low MC and CD = 0 ps/nm, (b) moderate MC and CD = 500 ps/nm, and (c) high MC and CD = 1000 ps/nm.

where r_{core} is the core radius and d is the distance between core centers at the fiber joint.

B. IN-PHASE QUADRATURE HISTOGRAM (IQH)

The IQH provides statistical features for both amplitude and phase of the received signal. In Fig. 4, we show the IQH using two-dimensional representation, where the x-axis and y-axis denote the amplitude of the I and Q components, respectively, and z-axis denotes the number of occurrences of each (x,y) combination. In Fig. 4 (a), we show the IQH of QPSK, 16-QAM and 64-QAM with low MC and CD = 0 ps/nm. It is clear that the three modulation formats have obvious differences. Fig. 4 (b) shows the effect of moderate MC and CD = 500 ps/nm. We notice that the IQH points begin to overlap, and this is apparent for the 64-QAM constellation. The effect of high MC and CD = 1000 ps/nm makes it difficult to distinguish between 16-QAM and 64-QAM, as shown in Fig. 4 (c). However, it is expected that the IQH improves the MFI performance accuracy in comparison with the one-dimensional methods such as the AAH [14].

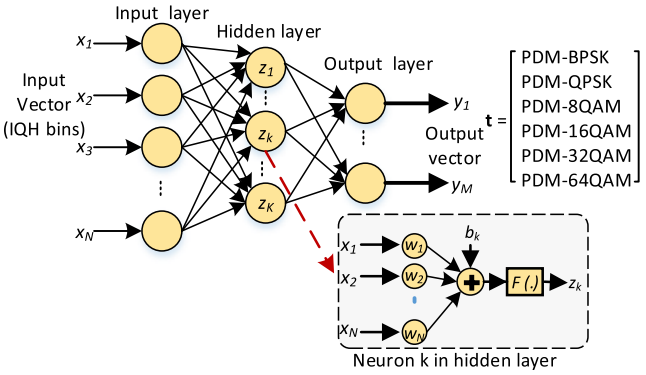

FIGURE 5. The ANN structure for MFI using IQH as input and modulation format as output.

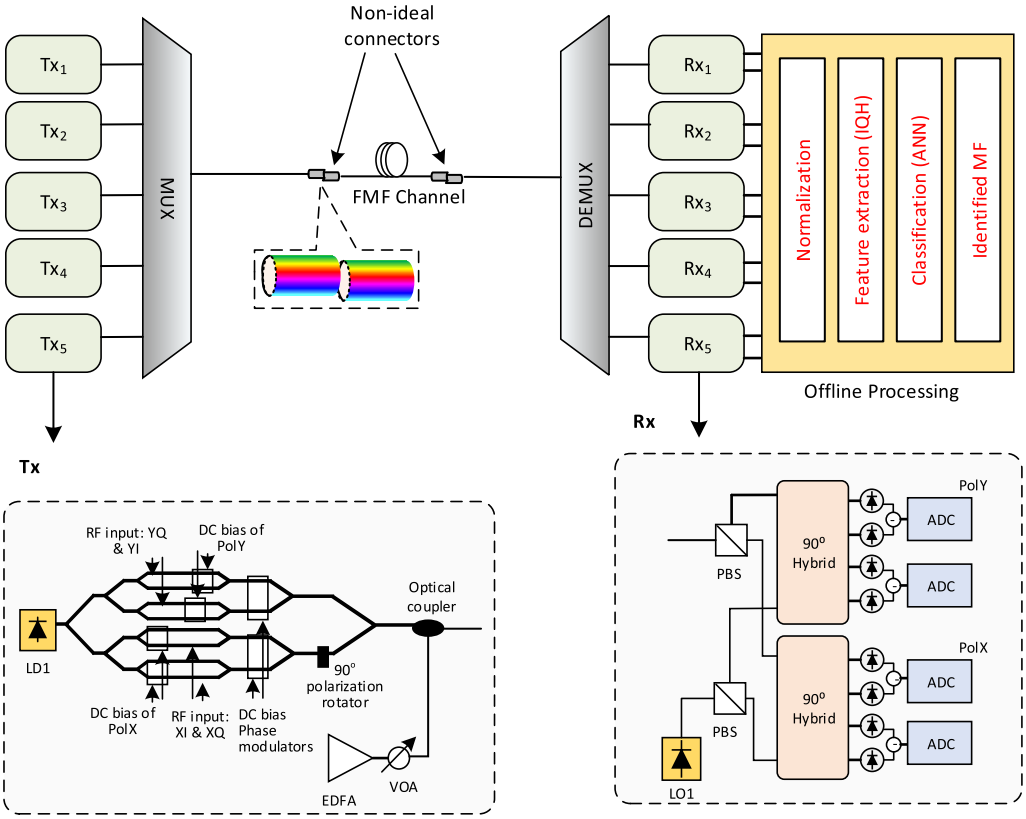

FIGURE 6. Simulation setup of the proposed FMF-MFI system. LD: laser diode, RF: radio frequency, EDFA: Erbium-doped fiber amplifier, VOA: variable optical attenuator, MUX: multiplexer, DE MUX: de- multiplexer, FMF: few mode fiber, PBS: polarization beam splitter, ADC: analog to digital convertor, LO: local oscillator, ANN: artificial neural network, IQH: in-phase quadrature histogram, MF: modulation format.

C. MFI USING ANN TRAINED WITH IQH

In this work, we exploit the IQH in conjunction with the ANN for the identification of M-QAM and M-PSK modulation formats in coherent FMF optical transmission systems. The IQH matrix can be expressed as a $1\times N$ vector $\mathbf{x}$. This vector is used as an input to the ANN. The elements of the ANN are modeled by a bias, set of weight coefficients, and an activation function, called neuron. The ANN architecture comprises three layers of neurons: the input layer, one or more hidden layers, and an output layer, as shown in Fig. 5. The input layer accepts an input vector $\mathbf{x}$, then transfers the vector samples to all neurons of the hidden layer (i.e. 20 neurons in this work). The connection between the layers is done by the network weights. The computation that occurs in the k^{th} neuron is calculated as

$$z_k = F\left(\sum_{i=1}^{N} w_{ik}\, x_i + b_k\right), \tag{6}$$

where $F(.)$ is the activation function, b_k is the bias of neuron k, and w_{ik}, $i = (1, 2, \ldots N)$, is the weighted connection at neuron k. We have used the sigmoid activation function given by

$$F(\alpha) = \frac{1}{1 - e^{-\alpha}}. \tag{7}$$

The ANN output can be expressed as

$$y_m = F\left(\sum_{j=1}^{K} w_{jm}\, z_j\right), \tag{8}$$

where y_m is the m^{th} network output, $m \in (1, 2 \ldots M)$, where M represents the number of modulation formats (i.e. $M = 6$ in our case). Each input vector $\mathbf{x}$ corresponds to a binary $1\times M$ vector t (i.e. target vector). The target vector has only one non-zero element where its position specifies the type of modulation. The error between the vectors $\mathbf{y}$ and $\mathbf{t}$ is calculated using the cross entropy loss function (L), which is proper for multiclass classification, given by [34]

$$L = -\frac{1}{M}\sum_{i=1}^{M} t_i\, log(y_i). \tag{9}$$

The loss (L) is back-propagated to optimize the network weights and bias during the training phase. We consider the scaled conjugate gradient algorithm [35] as an optimization algorithm. The training phase stops when L reaches a specified margin (i.e. 1×10^{-6}). In the testing phase, the type of modulation format is determined by argmax($\mathbf{y}$).

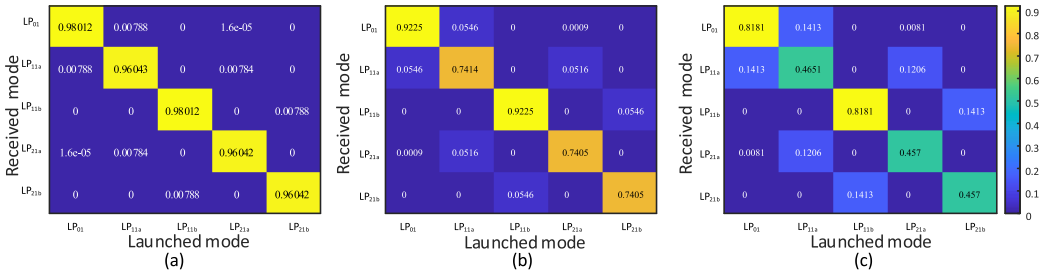

FIGURE 7. Mode coupling matrices of the five spatial modes: (a) MC_L at ($D_1 = 0.05$ and $D_2 = 0.05$), (b) MC_M at ($D_1 = 0.15$ and $D_2 = 0.15$), and (c) MC_H at ($D_1 = 0.25$ and $D_2 = 0.25$).

TABLE 1. Physical properties of FMF channel.

Name	Value
Dispersion	LP_{01}: 21.1 (ps/nm.km) LP_{11}: 22.0 (ps/nm.km) LP_{21}: 21.4 (ps/nm.km)
Dispersion slope	LP_{01}: 0.066 (nm^2.km) LP_{11}: 0.064 (nm^2.km) LP_{21}: 0.056 (nm^2.km))
Differential group delay (DGD)	LP_{11}-LP_{01}: 2.00 ps/m LP_{21}-LP_{01}: 3.90 ps/m

TABLE 2. Impairments values used in simulation.

Impairment	Value
OSNR	8–38 dB
LD linewidth	100 KHz
CD	LP_{01}: 0, 527.5, and 1055 (ps/nm) LP_{11}: 0, 550.0, and 1100 (ps/nm) LP_{21}: 0, 553.5, and 1070 (ps/nm)
MC (as a function of D for connectors 1 and 2)	MC_L: ($D_1 = 0.05$ and $D_2 = 0.05$) MC_M: ($D_1 = 0.15$ and $D_2 = 0.15$) MC_H: ($D_1 = 0.25$ and $D_2 = 0.25$)

III. SIMULATION SETUP

The simulation setup of the FMF transmission system is built using *VPITransmissionMaker*^{TM}9.9 simulator, as shown in Fig. 6.

At each transmitter block (see Fig. 6(a)), six PDM-modulation formats i.e. PDM-BPSK, PDM-QPSK, PDM-8QAM, PDM-16QAM, PDM-32QAM, and PDM-64QAM) are generated at various system speeds 10, 14, and 20 Gbaud. A 1550 nm laser diode (LD) with 100 KHz linewidth is used as a signal source at each transmitter. The ASE noise is added using an erbium-doped fiber amplifier (EDFA), while a variable optical attenuator (VOA) is used to change the OSNR value. Five spatial modes are considered in this work (i.e. LP_{01}, LP_{11a}, LP_{11b}, LP_{21a}, and LP_{21b}). A spatial multiplexer with five SMF inputs is utilized to produce a linear combination of the five spatial modes into an FMF channel. The FMF has a refractive index of step-index (SI) profile. In Table 1, we summarize the properties of a commercial FMF (OFS company) that is used in our system. Two non-ideal connecters with lateral misalignment, $D = 0.05$, 0.15, and 0.25, have been used to emulate the effect of MC.

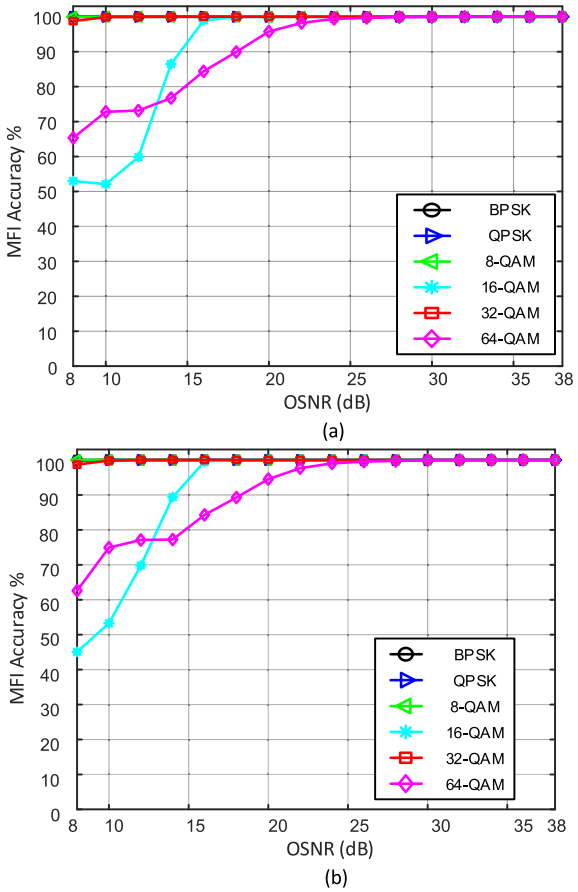

FIGURE 8. MFI accuracy vs OSNR at CD = 0 ps/nm in the presence of MC_L for (a) LP_{01} and (b) LP_{11a}.

In addition, the FMF length is varied in order to provide different values of CD. All the impairments' values are summarized in Table 2.

At the receiver, an FMF de-multiplexer is used to decouple the five spatial modes into five separate SMFs. For each receiver block (see Fig. 6(b)), a coherent receiver is employed to generate the recovered electrical signal of each mode. The resultant electrical I and Q signal' components, of each polarization, are sampled using two analog to digital converters (ADCs), where 8192 amplitude samples are obtained for each component. The normalized I and Q components form an IQH matrix of 80 × 80 bins. The IQH matrix is reshaped to

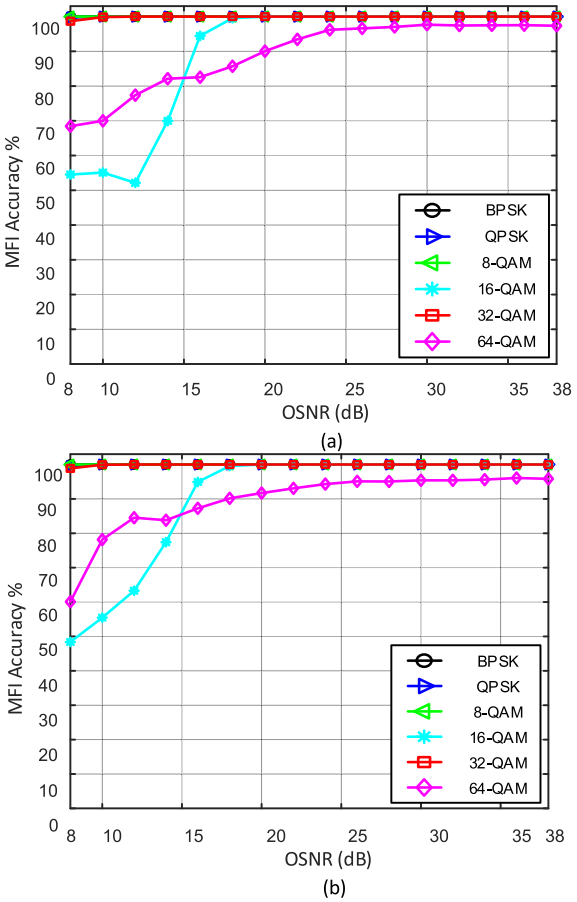

FIGURE 9. MFI accuracy vs OSNR in the presence of MC_M over dispersive channel for (a) LP_{01} when CD = 527.5 ps/nm, (b) LP_{11a} when CD = 550 ps/nm.

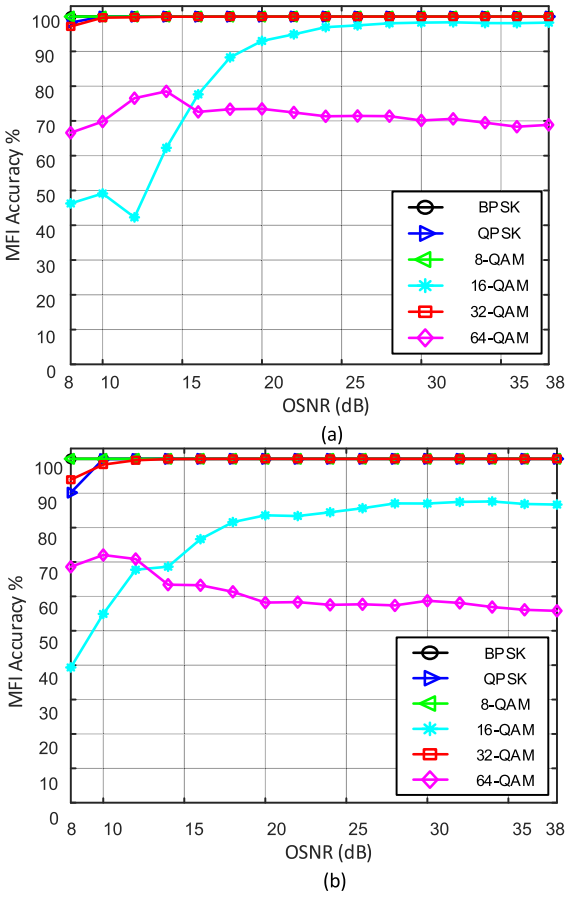

FIGURE 10. MFI accuracy vs OSNR in the presence of MC_H over dispersive channel for (a) LP_{01} when CD = 1050 ps/nm, (b) LP_{11a} when CD = 1100 ps/nm.

generate a 1-D vector. The 1-D vector is then applied as an input to the ANN.

IV. RESULTS AND DISCUSSION

In this section, we discuss the MFI accuracy results for the FMF-based optical network. It is worthy to mention here that the MC matrices are obtained according to [29]. The MC matrix for three kinds of lateral misalignment is shown in Fig. 7. It is clear from Fig. 7 that the self-coupling (diagonal) coefficients of LP_{01} and LP_{11b} modes are equal. Also, the self-coupling coefficients of LP_{11a}, LP_{21a} and LP_{21b} modes are equal. And because the off-diagonal elements of coupling matrices are relatively small, we show in this study the MFI results of LP_{01} and LP_{11a} only to avoid redundancy. We discuss the identification results as a function of the OSNR in the coexistence of all MC and CD values shown in Table 2. This generates 9 different combinations of MC and CD impairments. For each case, we generate 9600 data set size (i.e. 100 realizations $\times$16 OSNR values $\times$ 6 modulation schemes). The ANN is trained using 70% of the total data set size, while 30% is used for testing. In the following, we show the identification accuracy results for three MC-CD combinations at 10 Gbaud network transmission speed. In Fig. 8, we show the MFI accuracy at CD = 0 ps/nm and in the coexistence of low lateral misalignment (i.e. MC_L) for LP_{01} and LP_{11a}, at different OSNR values. The classification accuracy reaches 100% for the six modulation formats at OSNR values $\geq$24 dB for LP_{01} and LP_{11a} modes. At low OSNR values, the 64-QAM is most likely to be classified as 16-QAM due to the similarity of both constellations as noise level increases.

The MFI accuracy versus OSNR values in the coexistence of moderate lateral misalignment (i.e. MC_M) and CD = 527.5 (550) ps/nm for LP_{01} (LP_{11a}), is shown in Fig. 9. For LP_{01} (LP_{11a}) mode, the classification accuracy is 100% for BPSK, QPSK, 8-QAM, and 32-QAM. However, it reaches 100% for 16-QAM at 18 dB OSNR for LP01 and LP11a modes. For 64-QAM, the MFI accuracy achieves $\sim$ 98% and $\sim$ 96% for LP_{01} and LP_{11a}, respectively, at 24 dB OSNR. This can be justified by the difference in the self-coupling coefficients of both modes, see Fig. 7. For high lateral misalignment (i.e. MC_H), Fig. 10 shows the identification accuracy for LP_{01} and LP_{11a} at CD equal to 1055 and 1100 ps/nm, respectively. The identification accuracy of 64-QAM reduces to 70% (58%) in case of LP_{01} (LP_{11a}) for OSNR values greater than 20 dB. The reason of this performance is owing to the high MC and CD effects which cause the 64-QAM constellation points to

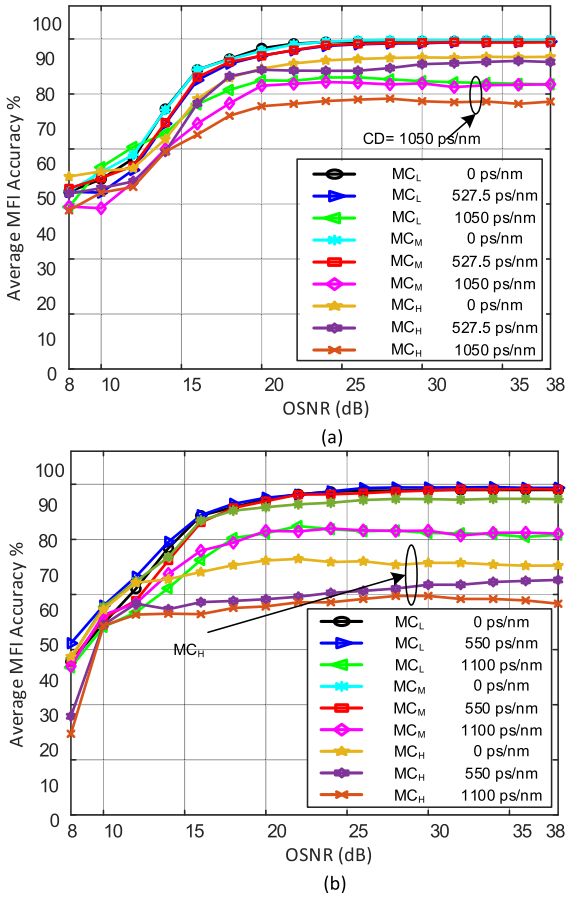

FIGURE 11. Average MFI accuracy vs OSNR value in the presence of all combinations MC and CD values: (a) LP_{01} and (b) LP_{11a}.

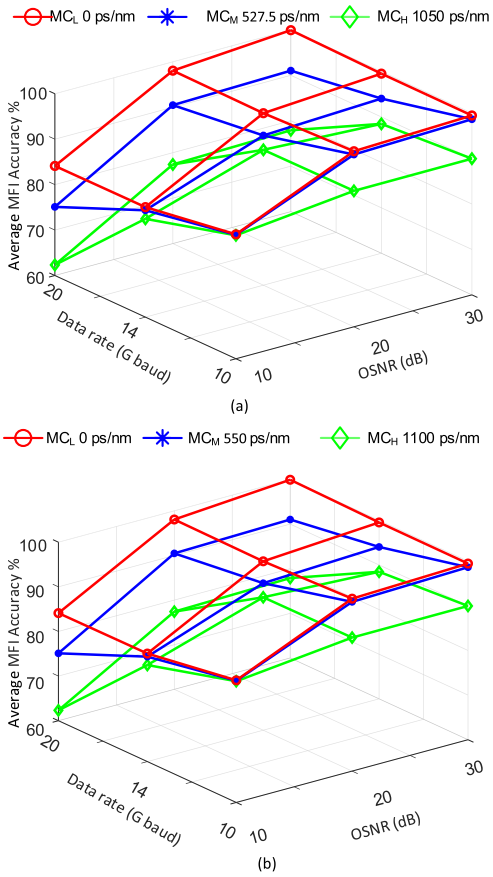

FIGURE 12. Average MFI accuracy at different data rate, OSNR, CD and MC: (a) LP_{01} and (b) LP_{11a}.

be closer to each other, making it difficult to identify this type of modulation, see Fig. 4 (c).

It is observed that there is an overlap between 16-QAM and 64-QAM for low and high OSNR values. In Fig. 11, we show the average identification accuracy versus OSNR values for all MC and CD combinations, for both LP_{01} and LP_{11a} modes. It is observed that the accuracy of LP_{01} is affected more by CD, while for LP_{11a} the dominant effect is due to the high MC. This can be explained by the low value of the self-coupling coefficients, shown in Fig. 7(c), which causes more than half of power to be coupled to the other modes. The investigation of the average MFI accuracy at 10, 14, and 20 Gbaud transmission speeds is also shown in Fig. 12. Three cases of MC and CD (i.e. MC_L-CD = 0 ps/nm, MC_M-CD = 527.5 (550) ps/nm, and MC_H-CD = 1050(1100) ps/nm) are considered under the transmission of LP_{01} (LP_{11a}) modes. For the first case, the average accuracy is greater than 98%, for both modes, when the OSNR value is greater than 20 dB, at the different transmission speeds. In the second case, the average accuracy reaches 90%, for both modes, at the highest transmission speed (i.e. 20 Gbaud), for OSNR greater than 20 dB. For the third case, the accuracy reduces to 80% and 78% at 20 Gbaud for LP_{01} and LP_{11a}, respectively, for OSNR greater than 20 dB.This is intuitively not surprising because the impact of CD rises, as system speed increases [36].

V. CONCLUSION

Existing literature have focused on modulation format identification in single-mode fiber. In this paper, we considered modulation format identification for few-mode fiber in optical networks for six commonly used types of PDM-QAM and PDM-PSK signals, and the transmission of five propagating spatial modes. The identification is achieved using features extracted from the in-phase quadrature histogram, along with the utilization of a feed-forward artificial neural network. The simulation investigation is assessed under mode coupling, chromatic dispersion, and amplified spontaneous emission for 10, 14, and 20 Gbaud transmission speeds. For low mode coupling and 20 dB OSNR, the average identification accuracies are greater than 98% for LP_{01} and LP_{11a}, and reduce from 98% to 90% when the speed changes from 10 to 20 Gbaud, at 20 dB OSNR. For the worst mode coupling (i.e. MC_H) and CD = 1100 ps/nm, the accuracies deteriorate to 80%(78%) for LP_{01}(LP_{11a}) at 20 dB OSNR. The implemented classification algorithm has the potential to be employed as a candidate in the future elastic FMF-based coherent optical networks.

REFERENCES

[1] R. Essiambre, G. Kramer, P. J. Winzer, G. J. Foschini, and B. Goebel, "Capacity limits of optical fiber networks," *J. Lightw. Technol.*, vol. 28, no. 4, pp. 662–701, Feb. 15, 2010.

[2] W. Klaus, B. J. Puttnam, R. S. Luís, J. Sakaguchi, J.-M. D. Mendinueta, Y. Awaji, and N. Wada, "Advanced space division multiplexing technologies for optical networks [Invited]," *IEEE/OSA J. Opt. Commun. Netw.*, vol. 9, no. 4, pp. C1–C11, Apr. 2017.

[3] D. J. Richardson, J. M. Fini, and L. E. Nelson, "Space-division multiplexing in optical fibres," *Nature Photon.*, vol. 7, no. 5, pp. 354–362, 2013.

[4] H. Chen, R. Van Uden, C. Okonkwo, and T. Koonen, "Compact spatial multiplexers for mode division multiplexing," *Opt. Express*, vol. 22, no. 26, pp. 31582–31594, 2014.

[5] G. Rademacher *et al.*, "159 Tbit/s C+L band transmission over 1045 km 3-mode graded-index few-mode fiber," in *Proc. Opt. Fiber Commun. Conf. Expo. (OFC)*, San Diego, CA, USA, 2018, pp. 1–3.

[6] Y. Wakayama, D. Soma, S. Beppu, S. Sumita, K. Igarashi, and T. Tsuritani, "266.1-Tbit/s transmission over 90.4-km 6-mode fiber with inline dual C+L-band 6-mode EDFA," *J. Lightw. Technol.*, vol. 37, no. 2, pp. 404–410, Jan. 15, 2019.

[7] D. A. B. Miller, "Reconfigurable add-drop multiplexer for spatial modes," *Opt. Express*, vol. 21, no. 17, pp. 20220–20229, 2013.

[8] X. Chen, A. Li, J. Ye, A. Al Amin, and W. Shieh, "Reception of mode-division multiplexed superchannel via few-mode compatible optical add/drop multiplexer," *Opt. Express*, vol. 20, no. 13, pp. 14302–14307, 2012.

[9] N. Amaya, S. Yan, M. Channegowda, B. R. Rofoee, Y. Shu, M. Rashidi, Y. Ou, E. Hugues-Salas, G. Zervas, R. Nejabati, D. Simeonidou, B. J. Puttnam, W. Klaus, J. Sakaguchi, T. Miyazawa, Y. Awaji, H. Harai, and N. Wada, "Software defined networking (SDN) over space division multiplexing (SDM) optical networks: Features, benefits and experimental demonstration," *Opt. Express*, vol. 22, no. 3, pp. 3638–3647, 2014.

[10] T. Tanaka, K. Pulverer, U. Häbel, C. Castro, M. Bohn, T. Mizuno, A. Isoda, K. Shibahara, T. Inui, and Y. Miyamoto, "Demonstration of single-mode multicore fiber transport network with crosstalk-aware in-service optical path control," *J. Lightw. Technol.*, vol. 36, no. 7, pp. 1451–1457, Apr. 1, 2017.

[11] V. A. J. M. Sleiffer, H. Chen, Y. Jung, P. Leoni, M. Kuschnerov, A. Simperler, H. Fabian, H. Schuh, F. Kub, D. J. Richardson, S. U. Alam, L. Grüner-Nielsen, Y. Sun, A. M. J. Koonen, and H. de Waardt, "Field demonstration of mode-division multiplexing upgrade scenarios on commercial networks," *Opt. Express*, vol. 21, no. 25, pp. 31036–31046, 2013.

[12] J. Xie, F. R. Yu, T. Huang, R. Xie, J. Liu, and Y. Liu, "A survey of machine learning techniques applied to software defined networking (SDN): Research issues and challenges," *IEEE Commun. Surveys Tuts.*, vol. 21, no. 1, pp. 393–430, 1st Quart., 2019.

[13] F. N. Khan, K. Zhong, X. Zhou, W. H. Al-Arashi, C. Yu, C. Lu, and A. P. T. Lau, "Joint OSNR monitoring and modulation format identification in digital coherent receivers using deep neural networks," *Opt. Express*, vol. 25, no. 15, pp. 17767–17776, 2017.

[14] L. Guesmi, A. M. Ragheb, H. Fathallah, and M. Menif, "Experimental demonstration of simultaneous modulation format/symbol rate identification and optical performance monitoring for coherent optical systems," *J. Lightw. Technol.*, vol. 36, no. 11, pp. 2230–2239, Jun. 1, 2018.

[15] F. N. Khan, K. Zhong, W. H. Al-Arashi, C. Yu, C. Lu, and A. P. T. Lau, "Modulation format identification in coherent receivers using deep machine learning," *IEEE Photon. Technol. Lett.*, vol. 28, no. 17, pp. 1886–1889, Sep. 1, 2016.

[16] X. Lin, Y. A. Eldemerdash, O. A. Dobre, S. Zhang, and C. Li, "Modulation classification using received signal's amplitude distribution for coherent receivers," *IEEE Photon. Technol. Lett.*, vol. 29, no. 21, pp. 1872–1875, Nov. 1, 2017.

[17] X. Lin, O. A. Dobre, T. M. N. Ngatched, Y. A. Eldemerdash, and C. Li, "Joint modulation classification and OSNR estimation enabled by support vector machine," *IEEE Photon. Technol. Lett.*, vol. 30, no. 24, pp. 2127–2130, Dec. 15, 2018.

[18] R. Borkowski, D. Zibar, A. Caballero, V. Arlunno, and I. T. Monroy, "Stokes space-based optical modulation format recognition for digital coherent receivers," *IEEE Photon. Technol. Lett.*, vol. 25, no. 21, pp. 2129–2132, Nov. 1, 2013.

[19] R. Boada, R. Borkowski, and I. T. Monroy, "Clustering algorithms for Stokes space modulation format recognition," *Opt. Express*, vol. 23, no. 12, pp. 15521–15531, 2015.

[20] D. Wang, M. Zhang, J. Li, Z. Li, J. Li, C. Song, and X. Chen, "Intelligent constellation diagram analyzer using convolutional neural network-based deep learning," *Opt. Express*, vol. 25, no. 15, pp. 17150–17166, 2017.

[21] D. Wang, M. Zhang, Z. Li, J. Li, M. Fu, Y. Cui, and X. Chen, "Modulation format recognition and OSNR estimation using CNN-based deep learning," *IEEE Photon. Technol. Lett.*, vol. 29, no. 19, pp. 1667–1670, Oct. 1, 2017.

[22] G. Liu, R. Proietti, K. Zhang, H. Lu, and S. B. Yoo, "Blind modulation format identification using nonlinear power transformation," *Opt. Express*, vol. 25, no. 25, pp. 30895–30904, 2017.

[23] J. Lu, Z. Tan, A. P. T. Lau, S. Fu, M. Tang, and C. Lu, "Modulation format identification assisted by sparse-fast-Fourier-transform for hitless flexible coherent transceivers," *Opt. Express*, vol. 27, no. 5, pp. 7072–7086, 2019.

[24] Z. Zhao, A. Yang, P. Guo, and W. Tang, "A modulation format identification method based on amplitude deviation analysis of received optical communication signal," *IEEE Photon. J.*, vol. 11, no. 1, Feb. 2019, Art. no. 7201807.

[25] Z. Zhao, A. Yang, and P. Guo, "A modulation format identification method based on information entropy analysis of received optical communication signal," *IEEE Access*, vol. 7, pp. 41492–41497, 2019.

[26] Q. Tan, A. Yang, and P. Guo, "Blind modulation format identification using differential phase and amplitude ratio," *IEEE Photon. J.*, vol. 11, no. 1, Feb. 2019, Art. no. 7201312.

[27] W. S. Saif, T. Alshawi, M. A. Esmail, A. Ragheb, and S. Alshebeili, "Separability of histogram based features for optical performance monitoring: An investigation using t-SNE technique," *IEEE Photon. J.*, vol. 11, no. 3, Jun. 2019, Art. no. 7203012.

[28] P. Sillard, M. Bigot-Astruc, and D. Molin, "Few-mode fibers for mode-division-multiplexed systems," *J. Lightw. Technol.*, vol. 32, no. 16, pp. 2824–2829, Aug. 15, 2014.

[29] J. Vuong, P. Ramantanis, Y. Frignac, M. Salsi, P. Genevaux, D. F. Bendimerad, and G. Charlet, "Mode coupling at connectors in mode-division multiplexed transmission over few-mode fiber," *Opt. Express*, vol. 23, no. 2, pp. 1438–1455, 2015.

[30] K.-P. Ho and J. M. Kahn, "Statistics of group delays in multimode fiber with strong mode coupling," *J. Lightw. Technol.*, vol. 29, no. 21, pp. 3119–3128, Nov. 1, 2011.

[31] R. Olshansky, "Mode coupling effects in graded-index optical fibers," *Appl. Opt.*, vol. 14, no. 4, pp. 935–945, 1975.

[32] S. Randel, R. Ryf, A. Sierra, P. J. Winzer, A. H. Gnauck, C. A. Bolle, R.-J. Essiambre, D. W. Peckham, A. McCurdy, and R. Lingle, "6×56-Gb/s mode-division multiplexed transmission over 33-km few-mode fiber enabled by 6×6 MIMO equalization," *Opt. Express*, vol. 19, no. 17, pp. 16697–16707, 2011.

[33] R. Ryf, S. Randel, A. H. Gnauck, C. Bolle, A. Sierra, S. Mumtaz, M. Esmaeelpour, E. C. Burrows, R.-J. Essiambre, P. J. Winzer, D. W. Peckham, A. H. McCurdy, and R. Lingle, "Mode-division multiplexing over 96 km of few-mode fiber using coherent 6×6 MIMO processing," *J. Lightw. Technol.*, vol. 30, no. 4, pp. 521–531, Feb. 15, 2012.

[34] S. S. Haykin, *Neural Networks and Learning Machines*. New York, NY, USA: Prentice Hall, 2009.

[35] M. F. Møller, "A scaled conjugate gradient algorithm for fast supervised learning," *Neural Netw.*, vol. 6, no. 4, pp. 525–533, Nov. 1993.

[36] I. Kaminow, T. Li, and A. E. Willner, *Optical Fiber Telecommunications VB: Systems and Networks*. Amsterdam, The Netherlands: Elsevier, 2010.

WADDAH S. SAIF received the B.Sc. degree in communication engineering from Hadhramout University, Hadhramout, Yemen, in 2003, and the M.S. degree in electrical engineering from King Saud University (KSU), in 2015, where he is currently pursuing the Ph.D. degree with the Electrical Engineering Department. Since 2010, he has been with the Electrical Engineering Department, KSU, as a Researcher/Graduate Student. His current research interests include optical CDMA, coherent optical receivers, performance monitoring of optical networks, and machine learning.

AMR M. RAGHEB received the B.S. (Hons.) and M.Sc. degrees from Tanta University, Egypt, in 2001 and 2007, respectively, and the Ph.D. degree from King Saud University, Riyadh, Saudi Arabia, in 2015, all in electrical engineering. He was a Teaching Assistant (TA) with Tanta University, from 2003 to 2008. He was a TA with King Saud University, from 2010 to 2015. He has over seven years of experience with the Photonics Telecommunication Laboratory. He is currently an Assistant Professor with King Saud University. His current research interests include photonic-microwave integration, quantum dash-based lasers, free-space optical communication, optical modulation format identification, coherent optical receivers, multiformat high-speed optical transmitter, and passive optical networks.

HUSSEIN E. SELEEM received the B.Sc. (Hons.) and M.Sc. degrees in electronics engineering and electrical communications from Tanta University, Tanta, Egypt, in 2001 and 2006, respectively, and the Ph.D. degree in electrical engineering from King Saud University (KSU), Riyadh, Saudi Arabia, in 2017. Since 2001, he has been with the Electronics Engineering and Electrical Communications Department, Tanta University, where he is currently an Assistant Professor. He was a Researcher with the Prince Sultan Advanced Technology Research Institute, KSU, in 2010, where he was mainly involved in optical and wireless communication projects. In 2012, he joined the Electrical Engineering Department, KSU, as a Researcher/Ph.D. Student, where he was involved in the area of wireless communications. His current research interest includes signal processing for wireless and optical communications.

TARIQ A. ALSHAWI received the M.S. degree in electrical engineering from the University of Michigan, Ann Arbor, MI, USA, and the Ph.D. degree from the Georgia Institute of Technology, Atlanta, GA, USA. He is currently an Assistant Professor with the Electrical Engineering Department, King Saud University, Riyadh. His current research interests include signal and image processing and human perception models, with applications in computer vision, bio-medical imaging, communication, and networks.

SALEH A. ALSHEBEILI was the Chairman of the Electrical Engineering Department, King Saud University, from 2001 to 2005. He has over 27 years of teaching and research experience in the area of communications and signal processing. He was a member of the Board of Directors with the King Abdullah Institute for Research and Consulting Studies, from 2007 to 2009, a member of the Board of Directors with the Prince Sultan Advanced Technologies Research Institute, from 2008 to 2017, where he was the Managing Director, from 2008 to 2011, and the Director of the Saudi-Telecom Research Chair, from 2008 to 2012. He has been the Director of the Technology Innovation Center, RF and Photonics in the e-Society, funded by the King Abdulaziz City for Science and Technology (KACST), since 2011. He is currently a Professor with the Electrical Engineering Department, King Saud University. He has been on the Editorial Board of the *Journal of Engineering Sciences*, King Saud University, from 2009 to 2012. He has also an active involvement in the review process of a number of research journals, KACST general directorate grants programs, and national and international symposiums and conferences.